Nuclear Inst. and Methods in Physics Research B 475 (2020) 8–13

Contents lists available at ScienceDirect

Nuclear Inst. and Methods in Physics Research B

journal homepage: www.elsevier.com/locate/nimb

Target K-shell X-ray emission associated with single and double electron capture for $F^{9+,8+,7+}$ + Ar collisions

D.S. La Mantia*, P.N.S. Kumara, J.A. Tanis

Western Michigan University, Kalamazoo, MI 49008 USA

ARTICLE INFO

Keywords:
Ions
Ion collisions
K shell
Ionization
Cross sections

ABSTRACT

Cross sections for target Ar K-shell ionization associated with single and double electron capture, as well as the same cross sections corresponding to projectile F K X-rays and the total cross sections for single and double capture, were determined for 1.8–2.2 MeV/u $F^{9+,8+,7+}$ projectiles. This work was performed at Western Michigan University using the tandem Van de Graaff accelerator. Coincidences between emitted X-rays and their corresponding charge-changed particles were detected. The Ar K X-ray coincidence cross section ratios for double to single capture are found to depend strongly on the incident charge state, with the ratios for F^{9+} well exceeding unity. Possible explanations for this anomalous behavior are discussed but a conclusive explanation is not found. The results are compared to previous experiments using fully-stripped fluorine where coincidence techniques were not employed.

1. Introduction

Ion-atom collisions provide a tool for the investigation of fundamental processes in atomic physics. This is especially true for the analysis of specific processes in which electrons are involved. The use of highly-stripped, swift ion projectiles and pure gaseous targets can isolate and enhance the results in many instances. Charge-changing cross sections and K-shell ionization are of particular importance in testing the validity of physical theories. K-shell ionization and electron capture have been the subject of many theoretical [1–3] and experimental [4,5] studies over the last half century.

The present investigation follows work done for fully-stripped fluorine [6,7] projectile ions on Ar targets using standard coincidence techniques that allow the assigning of emitted photons to the charge-changed particles emitting them. This enables the target or projectile X-rays to be associated with electron emission or, in this case, capture to the projectile ion. Previous investigations for fluorine on Ar [8,9] did not employ these techniques, or did so at significantly lower projectile velocities [10]. The total capture cross sections alone give no information about X-ray emission.

Swift projectile ions colliding with a neutral target can result in the loss of one or more electrons from the target. One or two of these electrons may come from the target K-shell, followed by the emission of a target K X-ray. In turn the projectile may capture any number of electrons. These captured electrons need not come from the target K shell. Cross sections for target X-ray emission with double and single electron capture, projectile X-rays with double and single capture, and total single and double electron capture were determined for 1.8–2.2 MeV/u $F^{9+,8+,7+}$ + Ar. The cross sections for target K-shell ionization by incident ions having zero, one, or two K-shell vacancies are found to have anomalies that cannot be easily understood in all cases.

2. Experimental procedure

This work was performed at Western Michigan University using the tandem Van de Graaff accelerator facility. Stripping gas at the accelerator terminal was used to create positive ions in charge state 7+. After exiting the accelerator, a 90° analyzing magnet was used to select F^{7+} ions with the desired energy. These ions could then be post-stripped to F^{8+} or F^{9+} by a thin carbon foil when required, with negligible loss to the beam energy. The desired ion beam was then deflected into the target beamline, focused using electromagnetic quadrupoles, and collimated by adjustable apertures before entering the interaction region (see Fig. 1).

The interaction region is a differentially-pumped gas cell 3.65 cm in length with entrance and exit aperture diameters of ~3 mm (the length of the cell has been adjusted for these apertures). The target gas pressure was measured using a capacitance manometer in a voltage feedback loop to control a valve on the chamber, setting the pressure in the cell to remain in the single-collision regime (total charge exchange less

* Corresponding author.
E-mail address: david.s.lamantia@wmich.edu (D.S. La Mantia).

https://doi.org/10.1016/j.nimb.2020.04.027
Received 29 January 2020; Received in revised form 21 April 2020; Accepted 22 April 2020

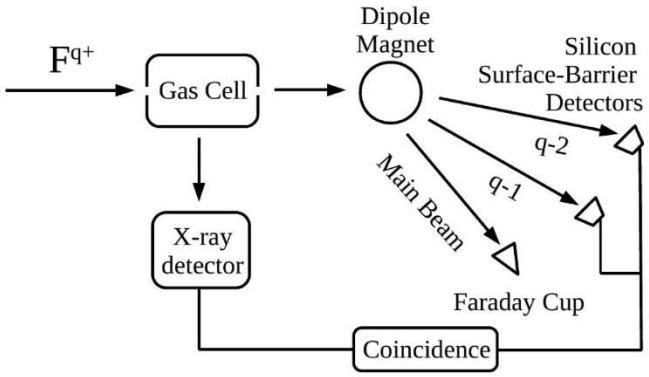

Fig. 1. Schematic for the projectile-target interaction region allowing the detection of emitted X-rays and charge-changed ions in coincidence.

than 5%). A Si(Li) x-ray detector with a 0.4 μm polymer window was placed at 90° to the beamline, with a detection efficiency of ~85% in the F K X-ray region and nearly 100% above 2 keV with an energy resolution (FWHM) of 157 eV at ~5.9 keV. The X-ray detector has an effective area of about 60 mm^2, with a beamline-to-crystal distance of ~17 mm.

After passing through the collision chamber, charge-changed and non-charge-changed beam components were separated using a dipole switching magnet. The primary projectile beam was collected by a Faraday cup biased to −200 V to suppress ejected electrons, measured with a Keithley electrometer, and then digitized to give the total number of incident particles not undergoing charge change.

The singly and doubly charge-changed beam components were observed using separate silicon surface barrier particle detectors with an efficiency of essentially unity. The X-ray and particle detector data were collected using an event-mode data acquisition system. Standard timing coincidence techniques were used to assign the emitted X-rays to their respective charge-changed particles, or vice versa.

Data were collected for F^{7+}, F^{8+}, and F^{9+} projectiles over the energy range 1.8–2.2 MeV/u at 8 mTorr Ar pressure. Also, data were collected at every point with no target gas to check the integrity of the coincidence system. The energy calibration for the X-ray spectra was performed using the Mn K_α and K_β lines from a standard ^{55}Fe source, as well as the hydrogen-like 1s-2p transition of fluorine [9].

Target and projectile K-X-ray emission, as well as total charge-changing, has been observed for F^{7+}, F^{8+}, and F^{9+} ions colliding with neutral target Ar gas. The scattered beam fraction (F) for one of these processes is given as the ratio of the number of events (X-rays or charge-changed particles) to the total incident beam. This fraction is a function of the target density (gas pressure P), and under single-collision conditions it is a linear function, i.e., F∝P. The fraction F is also necessarily proportional to the length of the gas cell. Following this, the differential electron capture cross sections are given as:

$$\left.\frac{d\sigma^{q-i}}{d\Omega}\right|_{\theta=90^\circ} = \frac{\Delta F}{\Delta P}\frac{1}{N_o L}\frac{1}{\epsilon\,\Delta\Omega}$$

where ΔF is the change in the scattered beam fraction for a given process, ΔP is the change in pressure associated with ΔF, N_o is the atomic (or molecular) gas density and is equal to $3.30*10^{13}$ [mT* cm^3]$^{-1}$, and L is the length of the cell. The effective gas cell length for the total capture cross sections was corrected by the geometrical factor $(a_1 + a_2)/\sqrt{2}$ [12], where a_1 and a_2 are the gas cell entrance and exit aperture diameters, respectively, to allow for the gas leaking out of the differentially pumped cell. For the X-ray cross sections, the detector efficiency and solid angle ΔΩ must also necessarily be included in the equation, where the solid angle ΔΩ is the detector area divided by the distance to the detector crystal squared (). The detector efficiency for Ar and F X-rays was taken to be 1.0 and 0.85, respectively. The fraction F was determined by measuring the number of charge-changed particles with electronic counters connected to the particle detectors, or photons counted with the X-ray detector, and dividing by the total number of incident particles obtained from the beam current and particle detectors.

The X-ray spectra were sorted by setting gates on the associated particle spectra to assign specific X-rays to singly and doubly charge-changed projectile ions. Examples of such sorted spectra are shown in Fig. 2. The Ar K_α and K_β lines can be seen centered at energies of about 3.3 and 3.7 keV, respectively. The Ar K_β/K_α relative intensity ratios for all the charge-state fluorine projectiles studied here are comparable to previously reported ratios averaged over a similar projectile energy range [8]. The F K X-ray peaks can also be seen in both the single capture (q-1) and double capture (q-2) spectra, with the q-2 F peak being slightly lower in energy than the q-1 F peak, as expected since the

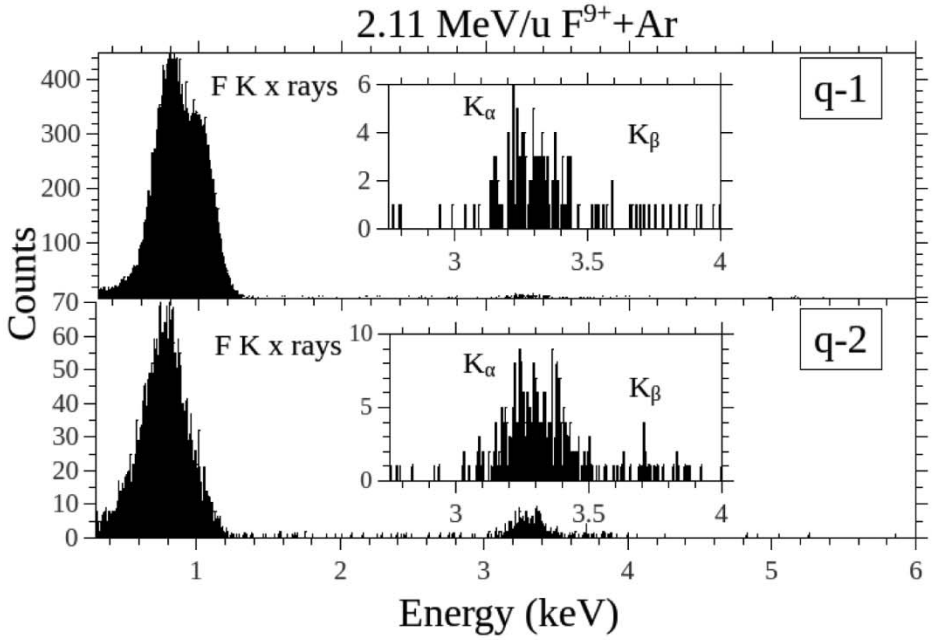

Fig. 2. 2.1 MeV/u F^{9+} + Ar (8 mTorr) coincidence X-ray spectra for single (q-1) and double (q-2) electron capture.

F q-2 ion has one more electron on it than F q-1.

The emission of target Ar K-shell X-rays caused by collisions with fluorine projectiles has been found to be nearly isotropic [11]; this finding will be assumed in this work. Integrating over the angular spherical coordinates therefore introduces a factor of 4π into the cross section equation for the total Ar K X-ray emission associated with electron capture.

In contrast, characteristic projectile F K X-ray emission has been shown to have a significant level of polarization (~23% for F^{9+} + Ar [11]). For an angular dependence of $\sin^2\theta$ in the F K X-ray differential cross section for anisotropic emission, integration introduces a factor of $8\pi/3$ in the total cross section. Taking the F K X-ray emission to be ~77% isotropic, following the observed polarization mentioned above would introduce an approximate factor of ~11.6 into the total cross section associated with characteristic projectile F K X-ray emission.

Systematic errors in the electronics include the uncertainty in the beam measurement from the Keithley electrometer (3%), the pressure accuracy from the capacitance manometer (5%), the physical dimensions of the gas cell (8%) and the X-ray and particle detectors mentioned above, and the counting of the charge-changed particles (< 2%). The differential pumping geometry of the gas cell has been taken into account for the total capture cross sections by including the geometrical correction, as discussed. The efficiency of the X-ray detector has been considered as discussed above, with a small effect on the cross sections for electron capture associated with F K X-ray emission and essentially no effect on the Ar X-ray emission cross sections. All of these systematic errors are much smaller than the relative counting errors for the cross sections.

3. Results

The cross sections for the charge-changing processes measured in this work are shown in Figs. 3–5, and the values are listed in Tables 1–3. The cross sections for Ar K-shell ionization associated with single electron capture are shown in the top panel of 3 and are reported in Table 1. An unexpected result is that these cross sections for F^{8+} are the largest, beginning at ~450 b and increasing quite strongly over the energy range to a final value of ~865 b. The cross sections for F^{9+} begin at nearly 85% of the F^{8+} values and also increase over the energy range,

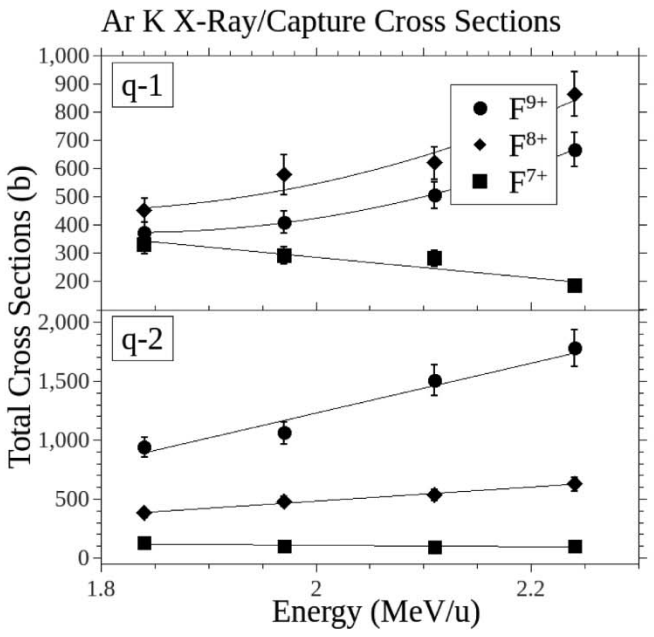

Fig. 3. Cross sections for target Ar K-shell ionization associated with single (q-1) and double (q-2) electron capture for $F^{7+,8+,9+}$ + Ar. The lines are drawn to guide the eye.

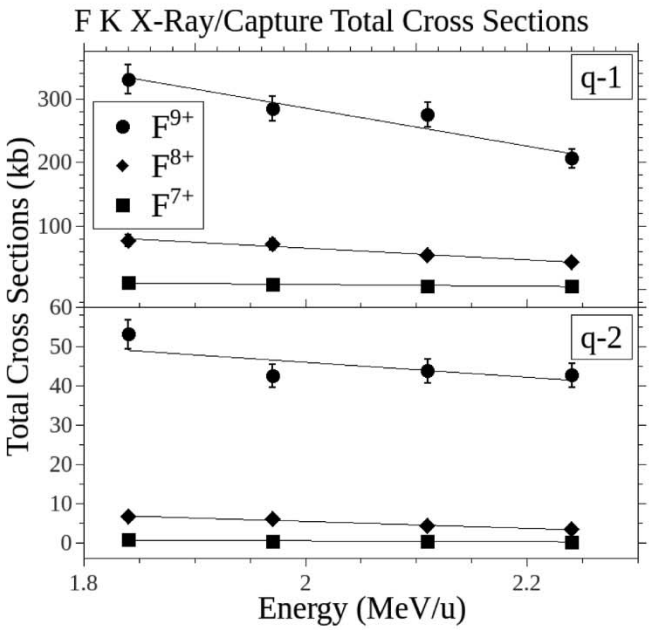

Fig. 4. Estimated total cross sections for projectile F K X-ray emission associated with single (q-1) and double (q-2) electron capture for $F^{7+,8+,9+}$ + Ar. The lines are drawn to guide the eye.

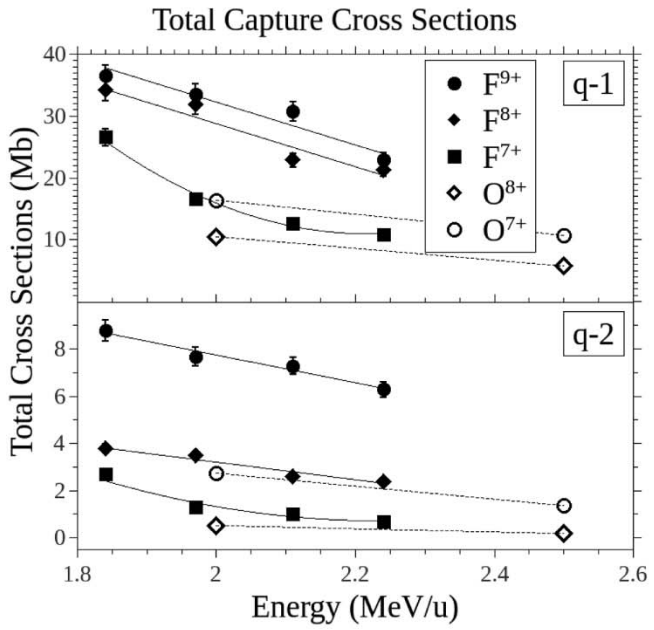

Fig. 5. Total single (q-1) and double (q-2) electron capture cross sections for $F^{7+,8+,9+}$ + Ar. Values for $O^{7+,8+}$ + Ar [12] (unfilled symbols) from an earlier work are also shown. The lines are drawn to guide the eye.

although not as strongly as those for F^{8+}, going to about 75% of the F^{8+} values. On the other hand, the F^{7+} cross sections decrease over the energy range, beginning at a comparable size to F^{9+} and decreasing by nearly a factor of 2.

The cross sections for Ar K-shell ionization associated with double electron capture are shown in the bottom panel of Fig. 3 and are also reported in Table 1. The F^{9+} cross sections are the largest, as expected, beginning at nearly 1 kb and increasing quite strongly over the energy range to ~1.8 kb. The F^{8+} double capture cross sections are nearly a factor of 3 smaller than those for F^{9+} and increase just slightly from ~400 b to ~600 b, a result that makes sense in view of the fact that to capture two electrons to F^{8+} requires one of the electrons to go to the L

Table 1
Cross sections (in barns) for target Ar K-shell ionization associated with double σ^{q-2}_{Ar-K} and single σ^{q-1}_{ArK} electron capture in the energy range 1.8–2.2 MeV/u for $F^{7+,8+,9+}$ + Ar. The average relative systematic uncertainties for these cross sections for all three charge-state projectiles are about 10%. Uncertainties in the final digit(s) is given in parentheses.

Projectile	Energy (MeV/u)	σ^{q-2}_{ArK}	σ^{q-1}_{ArK}
F^{7+}	1.8	128(15)	331(33)
	2.0	104(14)	291(30)
	2.1	96(13)	282(29)
	2.2	100(13)	186(21)
F^{8+}	1.8	382(37)	453(10)
	2.0	482(46)	579(7)
	2.1	536(50)	620(9)
	2.2	629(58)	865(9)
F^{9+}	1.8	941(85)	373(10)
	2.0	1064(95)	410(10)
	2.1	1508(131)	506(10)
	2.2	1782(155)	668(9)

Table 2
Differential cross sections for projectile F K X-ray emission associated with double $(\frac{d\sigma}{d\Omega})^{q-2}_{F-K}$ and single $(\frac{d\sigma}{d\Omega})^{q-1}_{F-K}$ electron capture (kb/sr) in the energy range 1.8–2.2 MeV/u for $F^{7+,8+,9+}$ + Ar. The average relative systematic uncertainties for the F^{7+}, F^{8+}, and F^{9+} cross sections are about 35%, 12%, and 7%, respectively. Uncertainty in the final digit(s) is given in parentheses.

Projectile	Energy (MeV/u)	$(\frac{d\sigma}{d\Omega})^{q-2}_{F-K}$	$(\frac{d\sigma}{d\Omega})^{q-1}_{F-K}$
F^{7+}	1.8	0.069(74)	1.0(3)
	2.0	0.036(54)	0.72(2)
	2.1	0.032(51)	0.57(2)
	2.2	0.020(40)	0.46(2)
F^{8+}	1.8	0.57(22)	6.7(7)
	2.0	0.53(21)	6.2(7)
	2.1	0.37(18)	4.7(6)
	2.2	0.29(15)	3.7(5)
F^{9+}	1.8	4.6(8)	29(3)
	2.0	3.7(7)	25(1)
	2.1	3.8(7)	24(1)
	2.2	3.7(7)	18(1)

Table 3
Cross sections (in Mb) for $F^{7+,8+,9+}$ + Ar total double σ^{q-2}_{TOT} and single σ^{q-1}_{TOT} electron capture for the energies studied. The average relative systematic uncertainties for these cross sections for all projectiles are about 5%. Uncertainty in the final digit(s) is given in the parentheses.

Projectile	Energy (MeV/u)	σ^{q-2}_{TOT}	σ^{q-1}_{TOT}
F^{7+}	1.8	2.7(1)	27(1)
	2.0	1.3(1)	17(1)
	2.1	1.0(1)	13(1)
	2.2	0.73(4)	11(1)
F^{8+}	1.8	3.8(2)	34(2)
	2.0	3.5(2)	32(2)
	2.1	2.6(1)	23(1)
	2.2	2.4(1)	21(1)
F^{9+}	1.8	8.8(4)	37(2)
	2.0	7.7(4)	34(2)
	2.1	6.3(4)	31(2)
	2.2	3.8(3)	23(1)

shell. The F^{7+} cross sections are a factor of 3 smaller than those for F^{8+} at the lowest energy and remain relatively constant over the energy range, but decrease slightly.

Of immediate note is that the Ar K-shell X-ray production cross sections associated with double electron capture for F^{9+} are more than twice those for single capture (see also Fig. 6), with both of those cross sections nearly doubling over the energy range. Also, it is noted that the projectile energy dependence of the cross sections associated with single and double capture for the F^{9+} and F^{8+} ions (but not F^{7+}) increase, a result that is contrary to typical capture cross sections (see Figs. 4 and 5). This suggests that these F^{9+} and F^{8+} cross sections are not primarily associated with capture but instead with ionization and excitation. In support of this, the double and single electron capture cross sections for the F^{9+} projectile associated with target Ar K X-ray production accounted for about 1% of the total target Ar K X-ray production [13]. The single and double capture cross sections associated with Ar K-shell X-ray production for F^{8+} are comparable to each other, with the double capture cross sections being slightly lower in value, and behave in essentially the same way over the energy range. The F^{7+} double capture cross sections begin at 40% of the value of the single capture cross sections and remain relatively constant, while the single capture cross sections decrease by about a factor of 2.

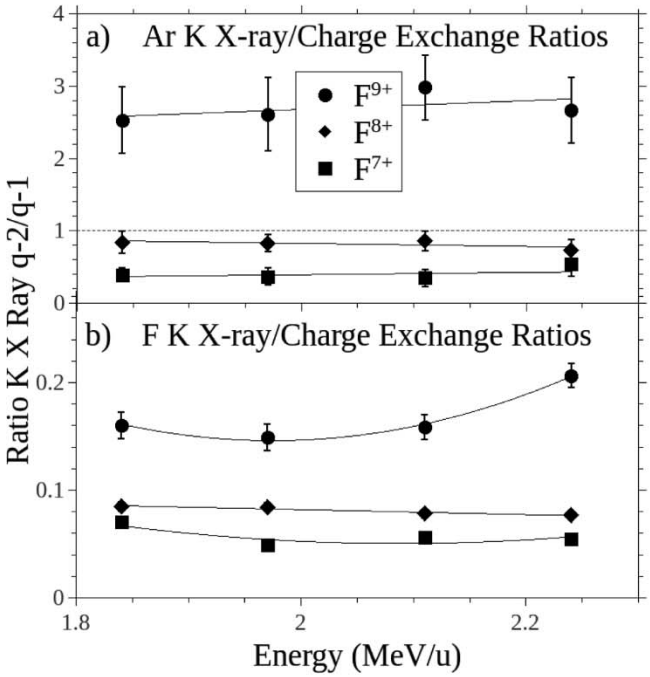

Fig. 6. Ratios (q-2/q-1) of double to single electron capture associated with a) target Ar K-shell ionization and b) projectile F K-shell X-ray production cross sections for F^{7+}, F^{8+}, and F^{9+} projectile ions. The average relative systematic uncertainties for the ratios for these projectiles are 30%, 20%, and 20%, respectively. The lines are drawn to guide the eye.

The differential cross sections for projectile F K X-ray emission associated with single electron capture are reported in Table 2. The estimated total cross sections for projectile F K X-ray emission associated with single capture were calculated using the ~23% polarization factor discussed previously are shown in the top panel of Fig. 4. The F^{9+} single capture differential cross sections are the largest as expected, beginning just below 30 kb and decreasing by about 40% over the energy range. The F^{8+} single capture differential cross sections are about a factor of 4 smaller than those for F^{9+} at the lowest energy and decrease over the energy range by nearly a factor of 2. The single capture F^{7+} differential cross sections begin at ~1 kb/sr and decrease over the energy range by a factor of 2. All of these cross sections decrease with energy as is typical for capture cross sections in this energy range.

The differential cross sections for projectile F K X-ray emission associated with double electron capture are also reported in Table 2. The estimated total cross sections for projectile F K X-ray emission associated with double capture calculated as mentioned above are shown in

the bottom panel of Fig. 4. The F^{9+} double capture differential cross sections begin just below 5 kb and exhibit a similar behavior to those for single capture, decreasing by ~25%. The differential cross sections for F^{8+} double capture are about 8 times smaller than those for F^{9+} and decrease by a factor of 2. The F K X-ray production differential cross sections for double capture for F^{7+} begin nearly an order of magnitude lower than those for F^{8+} and decrease by more than a factor of 3 over the energy range.

The total single electron capture cross sections are shown in the top panel of Fig. 5 and are reported in Table 3. The F^{9+} total single capture cross sections begin at ~37 Mb and decrease over the energy range by about 40% to ~23 Mb. The F^{8+} cross sections are comparable to those for F^{9+}, being a little smaller but behaving essentially the same way over the energy range studied. The F^{7+} cross sections start about 60% of those for F^{9+} and decrease more strongly than the F^{8+} and F^{9+} cross sections, beginning at ~27 Mb and decreasing by about 60% over the energy range.

The total double electron capture cross sections are shown in the bottom panel of Fig. 5 and are also reported in Table 3. These cross sections for all projectile charge states investigated do not decrease as strongly over the projectile energy range as do the single capture cross sections. The F^{9+} total double capture cross sections begin at ~9 Mb and decrease to ~4 Mb. The F^{8+} cross sections are about a factor of 2 smaller than those for F^{9+}, while the F^{7+} cross sections are comparable to those for F^{8+}, although somewhat smaller, and decrease by more than a factor of 3. These behaviors are expected, with the total capture cross sections decreasing with projectile energy and increasing with the projectile ionization state.

The F^{9+} total single capture cross sections are about a factor of four larger than those for double capture at the lowest energy studied, with this ratio increasing to about a factor of six over the energy range. For the fully-stripped projectile, it can be seen from Table 3 that the likelihood of double capture falls off more quickly than does single capture. The total double to single electron capture ratios for F^{8+} remain relatively constant at ~0.10, while those for F^{7+} decrease from ~0.10 to ~0.05 over the energy range, showing that double capture for F^{7+} falls off more quickly than does single capture.

4. Discussion

For the total cross sections (Fig. 5) the most significant difference between the single and double capture cross sections is the relationship of F^{8+} to the other projectile charge states. For single capture the F^{8+} cross sections are more comparable to F^{9+}, while for double capture they are more comparable to F^{7+}. This demonstrates the existence of a K-shell vacancy being the primary factor in the likelihood of electron capture. Both F^{8+} and F^{9+} can capture an electron to the K shell, while F^{7+} must capture to the L or a higher shell, and thus the total single electron capture cross sections for F^{8+} and F^{9+} are similar and considerably larger than those for F^{7+}. Only F^{9+} has two K-shell vacancies, making the likelihood of double electron capture larger than for F^{8+} and F^{7+}, which are more comparable.

These total single and double capture cross section results are comparable to those from earlier F^{q+} + Ar experiments [4,14] and are consistent with $O^{7+,8+}$ + Ar measurements performed over a similar energy range [12], also shown in Fig. 5. The F^{9+} cross sections are about a factor of 2 and 3 larger for single and double capture, respectively. The single capture cross sections for F^{8+} are about a factor of 3 larger than for O^{7+}, increasing to about 8 for double capture. These results are mainly due to the difference in charge state. The cross section results for Ar K X-ray emission associated with electron capture (Fig. 3) are more typical of ionization/excitation cross sections rather than total capture cross sections (Fig. 5), as seen in other ion-atom collision experiments [15,12].

The ratios of double to single electron capture (q-2/q-1) associated with target K-shell ionization are shown in Fig. 6a. It can be seen that the F^{7+} q-2/q-1 ratios for K-shell ionization are less than unity and stay relatively constant with projectile energy. The F^{8+} q-2/q-1 ratios are a little larger than those for F^{7+} and are close to, but never exceed, unity and are also relatively constant with energy. However, the F^{9+} q-2/q-1 ratios for K-shell X-ray emission well exceed unity and may increase slightly with energy. Since the projectile velocity is less than the average target K-shell velocity in this energy range, the likelihood of relative target K-shell ionization due to impact increases with projectile energy, while that of the total single and double electron capture decreases. This fact makes the present results somewhat unexpected.

In this energy range, the projectile velocity to target K-shell electron velocity ratio is about 0.6, while the projectile velocity to target L-shell electron velocity ratio is about 2. The more comparable the projectile to target K-shell velocities the more likely becomes capture from the K shell than from the L shell. The total Ar K X-ray cross sections from Ref. [8] and Ref. [16] are about 5 times greater than those reported here for single and double electron capture associated with Ar K-shell X-ray emission. This finding seems reasonable given that the major contributing factor to the Ar K X-ray cross section is impact-induced ionization without accompanying charge change [3]. It then follows that the likelihood of a K-shell electron being captured is relatively low. The Ar K X-ray cross sections do not show a decrease in magnitude as projectile energy increases, as do the total capture cross sections, instead increasing somewhat (see Figs. 3 and 5), following the behavior of impact-induced ionization with energy.

The ratios of double to single electron capture (q-2/q-1) associated with projectile F K-shell X-ray production are shown in Fig. 6b. As expected, all of these ratios are well below unity. The ratios for F^{8+} and F^{7+} are comparable over the energy range studied, with those for F^{8+} being slightly larger. These ratios also behave in essentially the same manner over the energy range, decreasing slightly. The ratios for F^{9+} are about double those for F^{8+} and may increase somewhat over the projectile energy range. However, this cannot be stated as a definite conclusion based on the one point being higher at the highest projectile energy studied.

As opposed to the cross sections for single electron capture associated with target Ar K ionization, those associated with projectile F K production certainly do not increase while being at least an order of magnitude larger across all projectile charge states. The double capture cross sections for F K X-ray production also do not increase as do those for Ar K-shell ionization, presumably due to electron capture being required for X-ray emission from a bare projectile which scales inversely with velocity in this energy region. The F K cross sections in the double capture case are, however, only factors of 2–6 larger than those for Ar K-shell ionization. Capture to a projectile with one (or two) K-shell vacancy may be accompanied by K-shell X-ray emission. For the F^{7+} projectile, with no K-shell vacancies, electron capture may occur along with the promotion of a K-shell electron, also resulting in the emission of a K X-ray. For highly-stripped fast ion projectiles at energies just slightly below the present work (1.4 MeV/u) colliding with Ar atoms, it has been shown that capture from the target L-shell dominates and target ionization is primarily from the L and M shells [17]. It is therefore reasonable that projectile F K X-ray production is far more likely than target Ar K-shell ionization.

5. Conclusion

The cross sections for single and double electron capture associated with target Ar K-shell ionization, the cross sections for single and double electron capture associated with projectile F K-shell X-ray emission, and the total single and double electron capture cross sections were determined for $F^{7+,8+,9+}$ projectiles in the energy range 1.8–2.2 MeV/u colliding with an Ar target. The total capture cross sections were found to decrease strongly with incident ion energy, as expected. The cross sections for capture accompanied by Ar K-shell ionization and F K-shell X-rays were determined using coincidence

techniques, allowing the charge-changed particles to be assigned to their respective emitted X-rays, and vice versa. All cross sections decreased as the number of initial bound projectile electrons increased with the notable exception of single capture associated with Ar K-shell ionization (Fig. 3).

The ratios of the double to single Ar K X-ray cross sections for F^{7+} were about 0.5 and did not vary greatly with incident projectile energy. These ratios for F^{8+} were a little below unity and also did not vary greatly with projectile energy. However, the ratios for F^{9+} well exceed unity with relatively constant values of ~2.5 over the energy range studied. This unexpected result gives insight into the importance of projectile K-shell vacancies in target X-ray production. The emission of target Ar K-shell X-rays is also directly correlated to the number of projectile K-shell vacancies. The presented results help to demonstrate the importance of projectile K-shell vacancies for capture processes.

CRediT authorship contribution statement

D.S. La Mantia: Conceptualization, Methodology, Software, Formal analysis, Investigation, Writing - original draft, Visualization, Project administration. **P.N.S. Kumara:** Software, Investigation. **J.A. Tanis:** Methodology, Validation, Investigation, Resources, Writing - review & editing, Visualization, Supervision, Funding acquisition.

Declaration of Competing Interest

The authors declare that they have no known competing financial interests or personal relationships that could have appeared to influence the work reported in this paper.

Acknowledgement

This work was supported in part by National Science Foundation Grant PHY-1707467.

References

[1] R.E. Olson, Phys. Rev. A 18 (1978) 2464.
[2] J. Eichler, F.T. Chan, Phys. Rev. A 20 (1979) 104.
[3] M.L. McKenzie, R.E. Olson, Phys. Rev. A 35 (1987) 2863.
[4] J.R. Macdonald, L. Winters, M.D. Brown, T. Chiao, L.D. Ellsworth, Phys. Rev. Lett. 29 (1972) 1291.
[5] T.R. Dillingham, J.R. Macdonald, P. Richard, Phys. Rev. A 24 (1981) 1237.
[6] D.S.L. Mantia, P.N.S. Kumara, A. Kayani, A. Simon, J.A. Tanis, Nucl. Instrum. Methods Phys. Res. B 408 (2017) 187.
[7] D.S. La Mantia, P.N.S. Kumara, A. Kayani, J.A. Tanis, X-Ray Spectrom. 1 (2019) 15.
[8] L.M. Winters, J.R. Macdonald, M.D. Brown, T. Chiao, L.D. Ellsworth, E.W. Pettua, Phys. Rev. A 8 (1973) 1835.
[9] F. Hopkins, R.L. Kauffman, C.W. Woods, P. Richard, Phys. Rev. A 9 (1974) 2413.
[10] J.R. Macdonald, C.L. Cocke, W.W. Eidson, Phys. Rev. Lett. 32 (1974) 648.
[11] J.H. Houck, P.A. Zavodszky, J.A. Tanis, Phys. Rev. A 56 (1997) 1954.
[12] E.H. Pedersen, S.J. Czuchlewski, M.D. Brown, L.D. Ellsworth, Phys. Rev. A 11 (1975) 1267.
[13] J.R. Macdonald, L.M. Winters, M.D. Brown, L.D. Ellsworth, T. Chiao, E.W. Pettus, Phys. Rev. Lett. 30 (1973) 251.
[14] S.M. Ferguson, J.R. Macdonald, T. Chiao, L.D. Ellsworth, S.A. Savoy, Phys. Rev. A 8 (1973) 2417.
[15] J.L. Forest, J.A. Tanis, S.M. Ferguson, R.R. Haar, K. Lifrieri, V.L. Plano, Phys. Rev. A 52 (1995) 350.
[16] S.J. Czuchlewski, J.R. Macdonald, L.D. Ellsworth, Phys. Rev. A 11 (1975) 1108.
[17] A. Muller, B. Schuch, W. Groh, E. Salzborn, H.F. Beyer, P.H. Mokler, R.E. Olson, Phys. Rev. A 33 (1986) 3010.